Sustainable Cities and Society 114 (2024) 105743

Contents lists available at ScienceDirect

Sustainable Cities and Society

journal homepage: www.elsevier.com/locate/scs

Extension and trend of the London urban heat island under Lamb weather types

Isidro A. Pérez [a,*], M. Ángeles García [a], Saeed Rasekhi [a], Fatemeh Pazoki [a], Beatriz Fernández-Duque [b]

[a] Department of Applied Physics, Faculty of Sciences, University of Valladolid, Paseo de Belén, 7, 47011 Valladolid, Spain
[b] Pyrenean Institute of Ecology, Spanish National Research Council (IPE-CSIC), Avda. Montañana, 1005, 50059 Zaragoza, Spain

ARTICLE INFO

Keywords:
Temperature field
Pressure field
Urban-rural
Temperature trend
Climate change

ABSTRACT

Understanding and describing how urban heat islands evolve is important, given the noticeable impact they have on people living in cities. This paper considers the London heat island from gridded values with one-arcminute spatial resolution over a 33-year period, from 1990 to 2022. Among the available variables in the database, maximum and minimum air temperatures were used. A cold island was not observed, since temperatures in the city centre were higher than those in the surroundings during the day and at night. However, the urban heat island extension was higher for the maximum temperature, whereas this island was limited to the city centre for the minimum temperature, in line with the area delimited by the congestion charge. Lamb weather types were determined, and it was found that the anticyclonic type prevailed, followed by southwest, west, and cyclonic types. The difference between both temperatures was about 6.8 °C in the city centre, and was particularly defined for anticyclonic and cyclonic types. Moreover, anticyclonic situations were linked with the highest urban heat island intensities for minimum temperature. Finally, the temperature trend was similar for both temperatures –about 0.2–0.3 °C/10 years in the city centre– thereby offering a possible quantification of climate change.

1. Introduction

The influence of urban areas on the environment and on inhabitants may be noticeable. This impact has been the subject of research over the last few years. Urban heat islands –i.e., the temperature contrast between the city centre and its surroundings– were barely investigated before 1990. However, the number of papers addressing this topic increased substantially, reaching over 300 in 2015 (Huang & Lu, 2018), and around 1000 articles in 2023, as recorded by Scopus (Elsevier, 2024). Interest in this topic may be attributed to the availability of information from satellite observations and to the recent development of gridded databases.

Mohan et al. (2022) divided the urban heat island effect into two categories; the first is the atmospheric urban heat island, while the second is the surface urban heat island. Zhou et al. (2018) conducted a historical review of the period 1972–2018 and found most research (69 %) to be focused on the daytime, whereas only 30 % of studies had investigated the urban heat island during the day and at night. An array of different methods has been suggested to identify this island. Some procedures are based on the contrast between the city centre and its surroundings. One example is Cetin et al. (2024), who used satellite images and took the difference between each pixel and the average temperature in rural areas. Si et al. (2024) considered the contrast between the urban area and its surroundings, which are less urbanised. Bala et al. (2024) used standardised temperatures, with the highest values being attributed to the urban heat island. Another experimental procedure is based on transect determination. Jaiswal et al. (2023) used a vehicle equipped with temperature and relative humidity sensors to investigate intra-urban thermal variability in Ahmedabad, India. In contrast to the previous methods, other procedures are statistical techniques, since observations are previously treated, as for example in Hu et al. (2022) or Yao et al. (2022), where a Gaussian function is used to smooth temperature values. The current paper falls into this latter line, although a nonparametric smoothing procedure was used, with the application of this procedure being one original contribution of the current paper to urban heat island research. Prior studies fitted various functions to quantify the contrast between the city centre and its outskirts. Sarker et al. (2024) used the inverse S-shaped function to fit the

* Corresponding author.
E-mail address: isidro.perez@uva.es (I.A. Pérez).

https://doi.org/10.1016/j.scs.2024.105743
Received 22 February 2024; Received in revised form 26 July 2024; Accepted 11 August 2024
Available online 16 August 2024

decline of urban land density from the city centre in Jakarta, Indonesia, with one feature of this procedure being that results do not consider different urban patterns following varied radial directions, since all of these directions are averaged. Fu et al. (2022) defined the urban city centre as the gravity centre of the built-up area, and the urban heat island effect was described by a single exponential decay model where all the directions are considered equally. If the aim is to examine the directional pattern, one possible procedure to be applied is that by Yang et al. (2022), who propose a model with a radial sweep where the gravity centre of an urban area is calculated and suggested as the origin for polar coordinates. North was the starting direction, and an exponential decay is used to scan land surface temperature and to establish the boundaries for the city influence.

One key concept is temperature difference, which is linked to the kind of urban development. If green spaces such as parks or green roofs are favoured, the cooling effect may counteract heating from buildings and pavements. However, meteorological conditions play a key role since, for instance, katabatic flow from nearby mountains may refresh the city during the night, or the urban heat island effect may prove prominent at sites under hot climates. Urban development managers should take the most suitable decision in order to ensure citizen well-being.

Remote sensing procedures have frequently been used. Mpakairi and Muvengwi (2019) used night-time lights as a proxy of anthropogenic activity in two urban cities of Zimbabwe, and highlighted the contribution of this variable to the summer night surface urban heat island. Similarly, Sun et al. (2020) estimated the urban heat islands of London and Paris from night-time light satellite imageries.

However, the values obtained may differ depending on the procedure used. Matuzko and Yakubailik (2018) studied the urban heat island in Krasnoyarsk, Russia, where the contrast between remote sensing measurements and those recorded by ground based stations exceeded 5 °C. This temperature contrast was also observed by Ravanelli et al. (2018) at the Georgia State University weather station, where data were compared to those from Landsat. Median temperature difference was 6 °C for 1992, and even the temperature trend was different, 0.08 °C/year for the weather station, and 0.22 °C/year for Landsat data.

New procedures have recently been developed and are awaiting application. Chau (2019) presented a method to estimate air temperature from smartphones in different contexts. Noticeable spatial resolution could be obtained using this method, which could be applied in urban heat island detection.

The variables involved in urban heat islands merit analysis by urban development managers in order to reduce the impact, since this island is affected by urban planning aspects such as population and road densities, land use mix, or percentage of open space, as well as landscape features such as shape complexity and compactness (Xu et al., 2019). Ridwan et al. (2021) established the relationship between urban heat islands and building density. Miles and Esau (2020) studied the surface urban heat island in 57 cities in northern Fennoscandia, which is formed by the Scandinavian peninsula, Finland, Karelia, and the Kola peninsula. They found a link between this island and population size in cities that had a more continental climate, with the intensity being greater for the larger cities, such as Murmansk and Oulu, and which ranged between 3 and 5 °C.

Urban heat island analysis may be an indicator of urban growth, with high resolution satellite images allowing for detailed analyses of specific areas. Karakuş (2019) used Landsat images with a resolution of 30, 60, 100 m to study the urban heat island in Sivas, Turkey. This analysis distinguished between urban built-up areas, vegetation, agricultural land, and barren land, and focused on three years –1989, 1999, and 2015. Moreover, an increase in urban built-up areas and urban heat island formation can be seen. Hamed Fahmy et al. (2023) detected an 18.9 % increase for the built-up area in the Sharqiyah region, Egypt, from satellite observations over the period 2001–2022. This change was accompanied by a temperature increase of about 4 °C.

Temperature distribution in urban areas is not only linked with physical features such as buildings or pavements, since economic activities also play a major role. City centres are the economic heart for regions –and even for countries– and are subject to intensive traffic and population displacement. Urbanization impact is a major problem in China where the temperature increase could be above 2 °C and where wind speed could decrease by up to 3 m s^{-1} (Wang et al., 2024). Moreover, gentrification processes are changing the city's social features, and can trigger changes and lead to urban restyling (Reades et al., 2022), with the urban heat island being sensitive to all these changes. The close link between an urban heat island and an urban pollution island was studied by Li et al. (2018) in Berlin, Germany. They observed an increase of about 12 % for surface urban heat island intensity at clear night due to the increase in absorbed radiation.

Although some variables are closely linked with urban environments and, in fact, some analyses focus on the urban pollution island, the contribution of meteorological variables should not be ignored. Shi and Zhang (2022) analysed the urban moisture island in Guangzhou, China, and obtained a daily evolution with a U-shape for the urban heat island, with a decrease after 6 h and an increase after 19 h. Li et al. (2020) studied the urban heat island in 419 major cities over the period 2003–2013 to investigate the most impacting variables, and highlighted not only vegetation activity and tree cover fraction but also temperature and precipitation. Alonso et al. (2007) analysed the urban heat island in Salamanca, a medium-sized Spanish city, and obtained values between −0.9 °C and 3.6 °C. Moreover, they considered the following three meteorological variables as the most contributing. The first was wind speed, since speeds above 6 m s^{-1} prevented the urban heat island from developing. Another variable was cloudiness, due to its link with the flux of incident solar radiation. Greater nocturnal urban heat island intensity was observed with high clouds. Finally, synoptic pressure conditions also contribute substantially, since the stability linked to anticyclonic situations favours more intense urban heat islands. However, instability situations determine a low intensity of urban heat islands.

The impact of synoptic situations on urban heat islands is the object of the current analysis. Buildings and their spacing modify the values of local meteorological variables. However, regional meteorological structures –such as pressure centres or air flow– have a regional dimension and might barely be affected by a city. Consequently, the interaction between local and regional structures merits inquiry and fills a gap in urban heat island research. The response of the urban heat island to the synoptic type should be investigated in order to establish the urban heat island spatial range and its intensity under regional meteorological features, so that correction measures can then be taken and future urban development planned in advance. This topic is studied in two ways, which are specific objectives of this paper. The first explores the relationship between the synoptic pattern and the urban shape. The second objective is to analyse the temporal evolution of the urban heat island. The selected city is London and the database used is extensive and dense enough to be employed in both spatial and temporal analyses. Among the various procedures available to determine the synoptic type, this paper considers the Lamb (1972) classification, following the Jenkinson and Collison (1977) method. The main advantage is its objective determination of weather type based on mean sea level pressure, which allows rapid determination of synoptic type with extensive databases. Three groups may be defined in this scheme, with the first being formed by directional flows following eight wind directions. The second group corresponds to situations governed by pressure centres such as cyclones or anticyclones, or their absence in unclassified situations. Finally, the third group considers hybrid situations where pressure centre features are mixed with directional flows.

Calculation procedures used for urban heat island and Lamb weather types are presented in the materials and methods section. The results section considers the maximum and minimum temperature distribution. The annual cycle is presented as a previous step for seasonal analysis. Among the various weather types, this paper focuses on the four most

frequent, and the contrast between the city centre and its surroundings is calculated. Finally, the temperature trend is analysed in order to quantify climate change impact in this city.

2. Materials and methods

2.1. Temperature database

The variables used were obtained from a gridded meteorological dataset for Europe (Thiemig et al., 2022). Spatial resolution was one arcminute, and the time range extended from 1990 to 2022. Although six variables are available at a daily resolution level, only the maximum and minimum temperatures, T_{max} and T_{min}, respectively, were used in this paper. The region studied is presented in Fig. 1 together with 3600 grid points where measurements are provided. Both spatial and temporal resolutions are sufficient for obtaining an initial approach to describing the urban heat island. However, specific hotspots are not observed with this database and their analysis would require an improved resolution. For instance, Seeberg et al. (2022) investigated the urban heat island in Stuttgart (Germany) with Landsat images at 30 m resolution. They attributed cooling spots to green roofs and albedo changes, whereas the sealing of surfaces was linked with warming spots. In the current study, the database provides robust results since the contribution of outliers is minimal when a sufficient number of observations is available.

Drivers of the urban heat island may be morphological, such as the building surface fraction or building heights, but also meteorological, such as air temperature or relative humidity. Finally, there are also socioeconomic drivers, such as the population or road density (Guan et al., 2023). There is a sharp socioeconomic contrast between the area spreading out to the southwest of the city centre and the area located northeast of the city centre, since the former is wealthier compared to the latter, where socioeconomic indicators such as child poverty, household income or life expectancy are worse (Hennig & Dorling, 2024). Most of the population lives in the city centre, where green spaces are common. However, a green belt surrounds the city at the boundaries of the greater London area, especially to the north and south (London Green Cover, 2024).

2.2. Determining the urban heat island

The following smoothing function was used (Donnelly et al., 2011):

$$T(x,y,h_1,h_2)=\frac{\sum_{i=1}^{N}K_1\left(\frac{x-x_i}{h_1}\right)K_2\left(\frac{y-y_i}{h_2}\right)T_i}{\sum_{i=1}^{N}K_1\left(\frac{x-x_i}{h_1}\right)K_2\left(\frac{y-y_i}{h_2}\right)}, \quad (1)$$

where T is temperature at point (x,y), T_i is the known temperature at point (x_i,y_i), K_i are the smoothing kernels, and h_i are the bandwidths. The kernel used was Gaussian

$$K(t)=(2\pi)^{-1/2}exp\left(-0.5z^2\right),\ -3<z<3. \quad (2)$$

The calculation interval was limited so as to increase calculation speed (Fernández-Duque et al., 2019). Silverman's method was used to calculate the bandwidth, h (Donnelly et al., 2011).

$$h=0.9\sigma n^{-1/5}, \quad (3)$$

where σ is the standard deviation of n data.

Once the temperatures had been smoothed, two urban heat island estimators were used. The first is the urban heat island index, UHII, which is defined at point i by

$$UHII_i=\frac{T_i-T'_{min}}{T'_{max}-T'_{min}} \quad (4)$$

where T_i is the temperature at one point in the region studied –shown in Fig. 1– and T'_{max} and T'_{min} are the maximum and minimum temperatures in this region. This index is a normalised quantity that represents the relative impact of the urban heat island on the study area, and which allows urban heat island intensity to be compared under different conditions. It has been used by several authors at different sites in India, such as Badugu et al. (2023) in their analysis for Tiruchilappalli, Mathew et al. (2017), who studied the urban heat island at Jaipur, or the research focused on Bengaluru, carried out by Suthar et al. (2023). The current study suggests a temperature associated with a UHII equal to 0.9, $T_{0.9}$.

However, Guha et al. (2018), and Hamed Fahmy et al. (2023) considered a less restrictive procedure since they considered the urban heat island at sites where temperature T_i is above a temperature threshold, T_T, following

$$T_i > T_T=\mu+0.5\cdot\delta \quad (5)$$

where μ is the mean, and δ the standard deviation of temperature in the studied region. This method was also followed in this paper, although it was considered an alternative procedure due to the greater extension of the urban heat islands obtained.

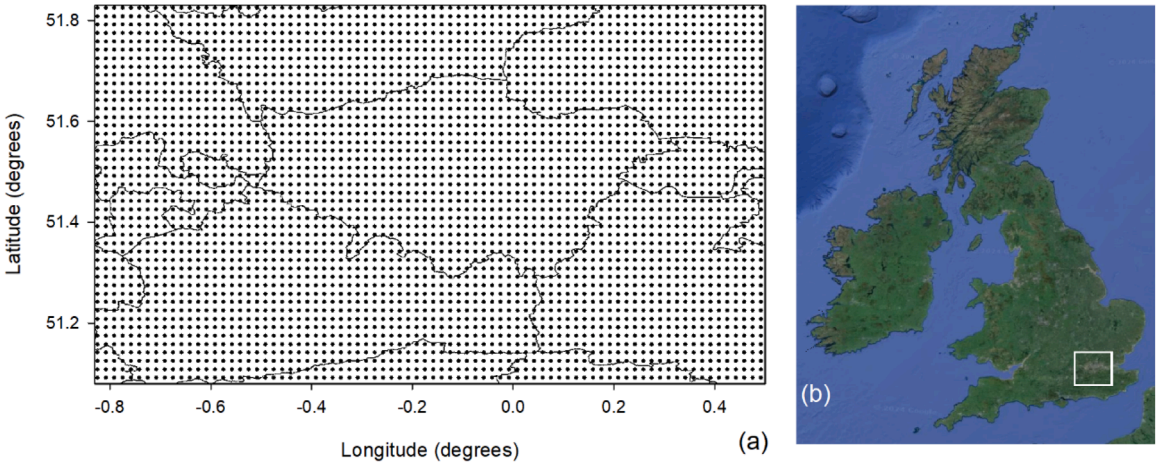

Fig. 1. (a) Study region and grid points where temperature data are available. (b) Analysed region in the British Isles from Google Earth.

2.3. Lamb weather types

Lamb weather types were calculated from pressure data obtained from NOAA (2024) using the objective procedure developed by Jenkinson and Collison (1977), where a 16-point spatial network is used. This is a reliable procedure to calculate the synoptic type since pressure changes at a continental scale are small. However, since a one-day temporal resolution is used, fast-moving small structures, such as small high-speed fronts may be inadvertently overlooked. The network centre was located at 0° E, 50° N, following Fig. 2.

The following expressions must be used with the corresponding sea level pressure values:

Westerly flow

$$W = \frac{1}{2}(P12 + P13) - \frac{1}{2}(P4 + P5) \tag{6}$$

Southerly flow

$$S = C1\left[\frac{1}{4}(P5 + 2 \times P9 + P13) - \frac{1}{4}(P4 + 2 \times P8 + P12)\right] \tag{7}$$

The resulting flow

$$F = \left(S^2 + W^2\right)^{1/2} \tag{8}$$

Westerly shear vorticity:

$$ZW = C2\left[\frac{1}{2}(P15 + P16) - \frac{1}{2}(P8 + P9)\right] - C3\left[\frac{1}{2}(P8 + P9) - \frac{1}{2}(P1 + P2)\right] \tag{9}$$

Southerly shear vorticity:

$$ZS = C4\left[\frac{1}{4}(P6 + 2 \times P10 + P14) - \frac{1}{4}(P5 + 2 \times P9 + P13) - \frac{1}{4}(P4 + 2 \times P8 + P12) + \frac{1}{4}(P3 + 2 \times P7 + P11)\right] \tag{10}$$

Total shear vorticity:

$$Z = ZW + ZS \tag{11}$$

where:

$$C1 = 1/\cos(latitude) \tag{12}$$

$$C2 = \frac{\sin(latitude)}{\sin(latitude - 5^{\circ})} \tag{13}$$

$$C3 = \frac{\sin(latitude)}{\sin(latitude + 5^{\circ})} \tag{14}$$

$$C4 = \frac{1}{2cos^2(latitude)} \tag{15}$$

Latitude is 50°N in this application.

$$Wind\ direction = tan^{-1}\left(\frac{W}{S}\right)\begin{cases} If\ W > 0\ and\ S < 0,\ add\ 360^{\circ} \\ If\ S > 0,\ add\ 180^{\circ} \end{cases} \tag{16}$$

Eight 45° sectors were used to determine wind direction.

A Lamb pure directional type appears if $|Z| < F$, i.e., northerly, N, north-easterly, NE, easterly, E, south-easterly, SE, southerly, S, south-westerly, SW, westerly, W, and north-westerly, NW.

The weather type is cyclonic, C, ($Z > 0$) or anticyclonic, A, ($Z < 0$), if $|Z| > 2F$.

The synoptic situation is a Lamb hybrid type if $F < |Z| < 2F$.

The pattern is the unclassified type, U, if $F < 6$ and $|Z| < 6$.

This classification gives 27 weather types.

2.4. Trend calculation

Annual temperature fields were obtained with Eq. (1) and linear trends were obtained for every point in Fig. 1. The statistical significance of the correlation coefficients was also calculated. Two specific significance levels were used, i.e., 1 % and 5 %.

Additionally, temperature distribution was calculated every day, and days with $T_{0.9}$ temperatures inside region borders were selected. A linear fit was first used. However, one drawback of the linear function is the intensive influence of outliers if the number of outliers is high. This drawback may be avoided by using a harmonic function. In a later step, $T_{0.9}$ was modelled following the equation formed by two parts, i.e., a linear part and a harmonic part, simplified from Pérez et al. (2017):

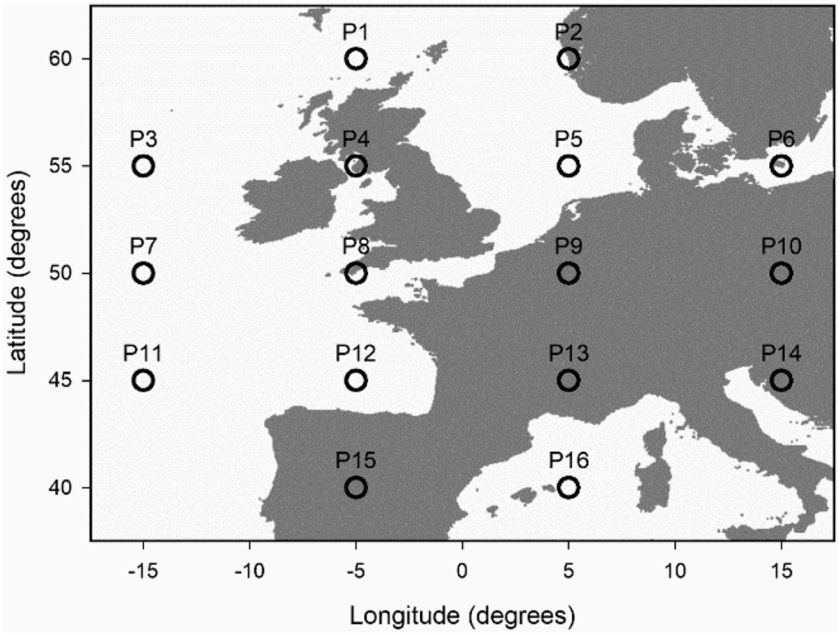

Fig. 2. Network used in the method of Jenkinson and Collison (1977) to determine Lamb weather types for the current analysis.

$$T_{0.9} = A + B\ t + C\ cos\left(\frac{2\pi t}{T}\right) + D\ sin\left(\frac{2\pi t}{T}\right) + E\ t\ cos\left(\frac{2\pi t}{T}\right) + F\ t\ sin\left(\frac{2\pi t}{T}\right), \quad (17)$$

where t is time, and T the period of one year. This model is based on the periodic pattern presented by the meteorological variables. Although fitted with a multiple linear function, the model represented by Eq. (17) is less sensitive to outliers due to the contribution of five terms depending on time. The most relevant feature of this model is that temperature trend is divided. One part corresponds to the B coefficient. However, the other part is obtained from the amplitude change with time, which is represented by a combination of harmonic terms.

3. Results

3.1. The urban heat island

Fig. 3. presents the urban heat island, which was calculated by smoothing all the observations with Eq. (1). T_{max} contrast was about 1.4 °C, and was slightly higher for T_{min}. The surface fraction whose temperature was above $T_{0.9}$ was 10.6 % for T_{max} and was longitudinally distributed. However, this surface fraction was 3.9 % for T_{min} and focused on the city centre. Moreover, surface expansion for lower temperatures, such as T_T, is longitudinal –along the river valley. The main feature is that the heat island is observed with both temperatures, especially with T_{min}. Since London is a city with abundant green spaces, the temperature contrast between the city centre and its surroundings is small. Moreover, the green belt is mainly located to the north and south of the city. This distribution justifies the latitudinal extension of the urban heat island. During the day, this island is the city's response to its activities and to solar heating, whereas the residual heat island is found in the city centre at the night. This heat centre may be the result of high urban density and may play a critical role under dangerous hot conditions (Zhou et al., 2024). Interactions between heat and urban pollution islands should be the subject of research since certain chemical reactions are favoured under high temperatures, for instance, ozone formation. Moreover, air pollutants, which are mainly found in the city centre and which can reduce visibility, determine longwave emission that favours the urban heat island effect.

3.2. The annual cycle

Monthly median temperature was calculated in the region where the values were smoothed, and is represented in Fig. 4. The mean difference between T_{max} and T_{min} is 6.9 °C, and thermal amplitude was 14.5 °C for T_{max} and 10.4 °C for T_{min}. Moreover, this cycle allows seasons to be defined, since winter is formed by the coldest temperatures, i.e. from December to February. Summer is formed by the hottest temperatures –from June to August– and the rest of the months are divided between both intermediate seasons, from March to May for spring, and from September to November for autumn.

3.3. Weather types

Lamb weather types were obtained and their frequencies were calculated and presented in Fig. 5. Prominent is A type, with a frequency close to 25 %. Other noticeable types are W, SW, and C. The frequency of these four types is near to 52 %. Consequently, the rest of the paper

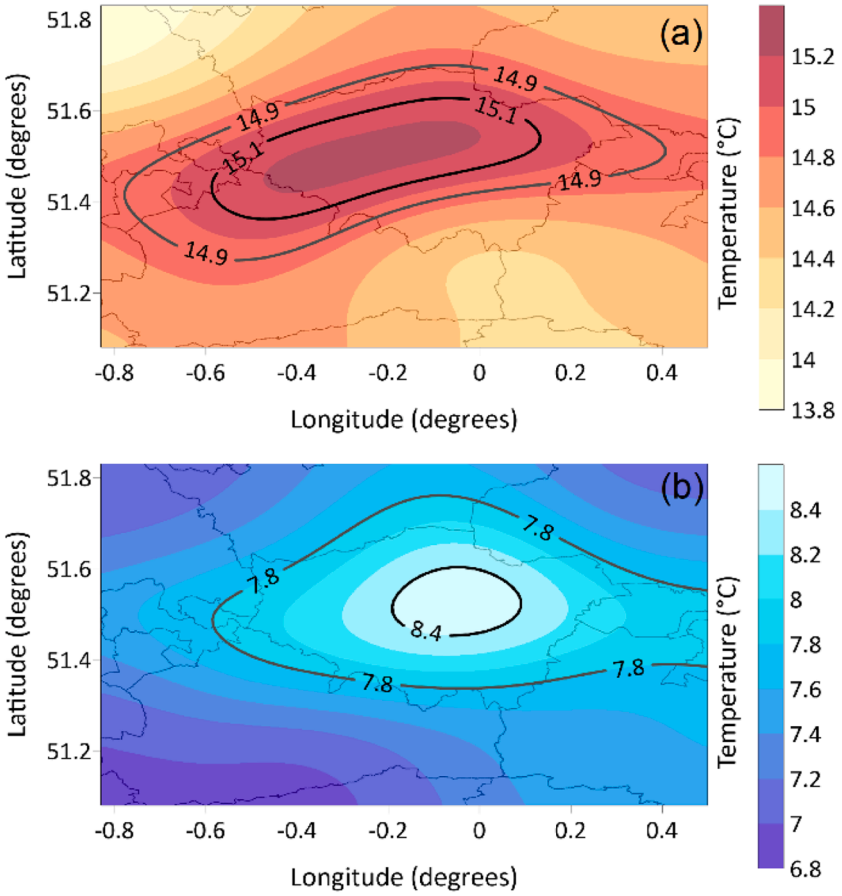

Fig. 3. Urban heat island for T_{max} temperatures (a) and T_{min} temperatures (b). The inner black line corresponds to $T_{0.9}$, the outer grey line to the temperature threshold, T_T.

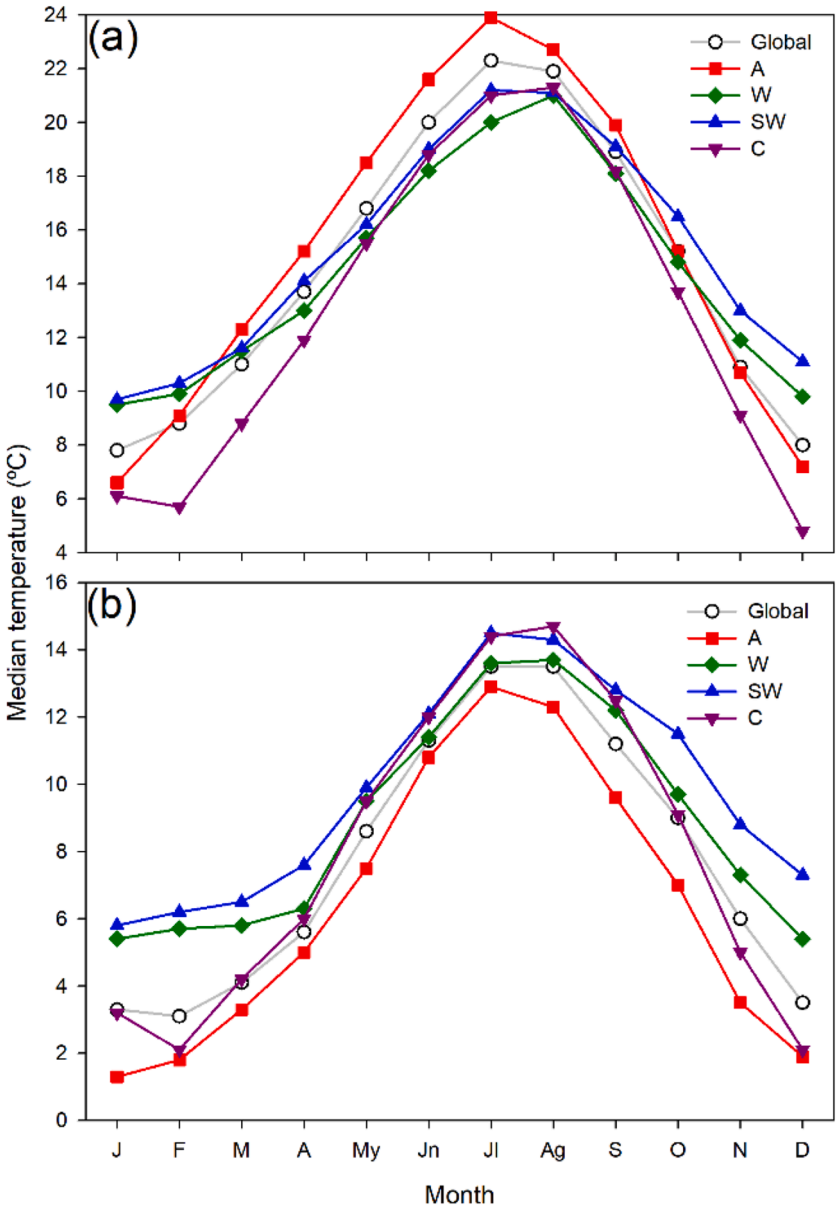

Fig. 4. Annual temperature cycle obtained from the median of smoothed values in the region (a) T_{max}, (b) T_{min}. Calculations were made with global observations and for the most representative weather types.

focuses on these types, since they are the most representative. Seasonal distribution of frequencies is also presented in Fig. 5, where A type peaks, especially in summer, when frequency was around 28 %. W and SW types were the next most frequent types in winter and autumn. However, C type was the second most frequent in spring, and U type was the third most frequent in summer.

Fig. 6 presents the isobar distribution, where the first row corresponds to a general description of the flow associated to the most frequent types. The pressure centres for A and C types are in the middle of the region presented in Fig. 2. Isobar orientation is the main difference between W and SW types, with the geostrophic wind flowing along these isobars. The highest wind speed is observed for the W type followed by the SW type, since the isobar spacing is narrower for the W type. The seasonal distribution of pressure fields is also presented. Key points in the annual evolution are the pressure values and the isobar spacing, which determines wind intensity. Wind speed is noticeable in winter for W and SW types, and the lowest values are obtained for the C type. Another feature that may be highlighted is the close link between the pressure field for all the observations and that for spring, which could be used instead of the pressure field from all the observations. For the A type, the highest pressure values were observed in winter (above 1028 hPa), compared to those obtained in summer, which were the lowest (below 1024 hPa). The opposite behaviour is observed for the C type, since the lowest values were below 1000 hPa in winter and above 1008 hPa in summer.

Fig. 4 presents the annual cycle for these types, where type A stands out due to the sharp contrast between the two temperatures, which is around 8.8 °C. Types W and SW are linked to mild temperatures. They are low for T_{max} and high for T_{min} in summer. However, this feature is particularly pronounced in the period January-March for T_{min}, since temperature remained steady and close to 6 °C. This result is justified by the air flow presented in Fig. 6, where the flow comes from the ocean for both types. Moreover, temperatures are higher for the SW type, since winds came from lower latitudes, where temperatures were higher. Finally, C type stood out due its low T_{max} in the period November-April.

Results for specific weather types and seasonal analysis are presented as supplementary material. The urban heat island for T_{max} is presented in Fig. S1 and $T_{0.9}$ indicates that the highest temperatures are found in a

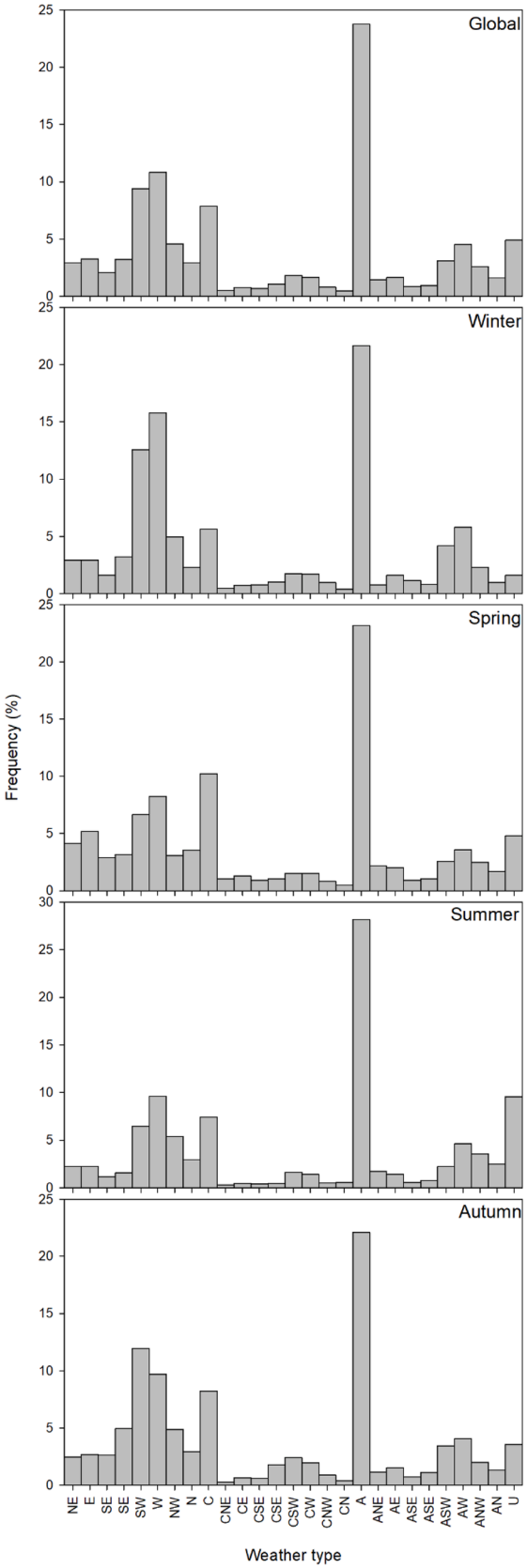

Fig. 5. Frequency distribution for global observations and for every season.

small region for A and C types, i.e., the highest temperatures are confined to the city centre for pressure centres located in the region studied. However, the extension of the highest temperatures is considerably greater and is directed towards the E for the W and SW types, i.e., W and SW directional flow triggers an increase in the urban heat island extension. The rest of the figure presents the seasonal pattern of temperatures under these weather types. The behaviour is quite similar, although the urban heat island spread towards the E for C type in autumn. For W types, the highest temperatures were confined to the city centre in spring, and in winter for the SW type. Differences between $T_{0.9}$ and T_T are quite small. However, the extension contrast may be noticeable. The highest extension for $T_{0.9}$ is for W type in autumn –around 19 %– whereas the lowest is for A type, also in autumn –around 7 %. Extension of the T_T region is higher, between 30 and 40 %. Both limits, $T_{0.9}$ and T_T, extended in longitude.

The T_{min} distribution is presented in Fig. S2. In this case, $T_{0.9}$ is confined to the city centre under all the situations studied, and only T_T extended beyond the boundaries investigated in approximately half of the cases; in particular, under W type, and summer and autumn for A and SW types. Surface for $T_{0.9}$ is between 3 % and 6 %, whereas for T_T it is between 28 % and 32 %. $T_{0.9}$ is close to the city centre, whereas T_T presents a longitudinal orientation.

Temperature difference T_{max}-T_{min} was calculated every day at every point of the grid, and all the values were smoothed with Eq. (1). The result is presented in Fig. 7. The lowest values were observed in the city centre and were about 6.8 °C. However, the greatest contrast was observed at SW, where the difference was over 1 °C higher than in the city centre. This calculation was made for the four most frequent weather types as well as seasonally. The result is presented in Fig. S3. A general result is the smallest contrast in the city centre, although the amount depends on weather type and season. Additionally, the contrast between the city centre and the surroundings is well defined under specific conditions; for instance, under A and C types, and for this last type in the seasonal analysis. Moreover, the largest contrasts are observed in the SW corner except for the SW type, where the most relevant contrasts were observed in the NE corner.

Table 1 presents the contrast between the average temperature in the region, with temperature above $T_{0.9}$, which is represented by T_{in}, and the average temperature outside this region, which is represented by T_{out}. Differences are around 0.5 °C for T_{max}, with T_{in} being greater than T_{out}. The highest contrast was 0.8 °C for the SW type in summer, and the lowest 0.4 °C for A and C types in autumn. The urban heat island intensified for T_{min}, since most differences were around 0.8 °C, although the highest contrasts were around 1.2 °C for most of the situations with A type.

3.4. Temperature trend

The slope of the linear fits for every point of the region studied from annual means is presented in Fig. 8. The significance levels of the correlation coefficients are also represented. T_{max} trends are positive in all the region. The highest values –around 0.4 °C/10 years– were observed in the east of the region. However, the trend in the city centre is about 0.2 or 0.3 °C/10 years. For T_{min}, the trend in the region may be both positive and negative. Positive values are below 0.4 °C/10 years and are observed in the city centre, with some being statistically significant at 5 % level. However, most of the negative values were observed in the southwest of the region, although they were not statistically significant.

Figure S4 presents the trend by weather type and season for T_{max}. In this case, the urban heat island is not observed. Moreover, values are only statistically significant at a level below 5 % with A type in most of the region. Under this type, the highest trend was about 0.7 °C in 10 years in the east of the region. Seasonal analysis presents noticeable results only for A type in winter when the trend in the city was around 0.5 °C in 10 years in the city centre. A similar result was obtained for W type in summer.

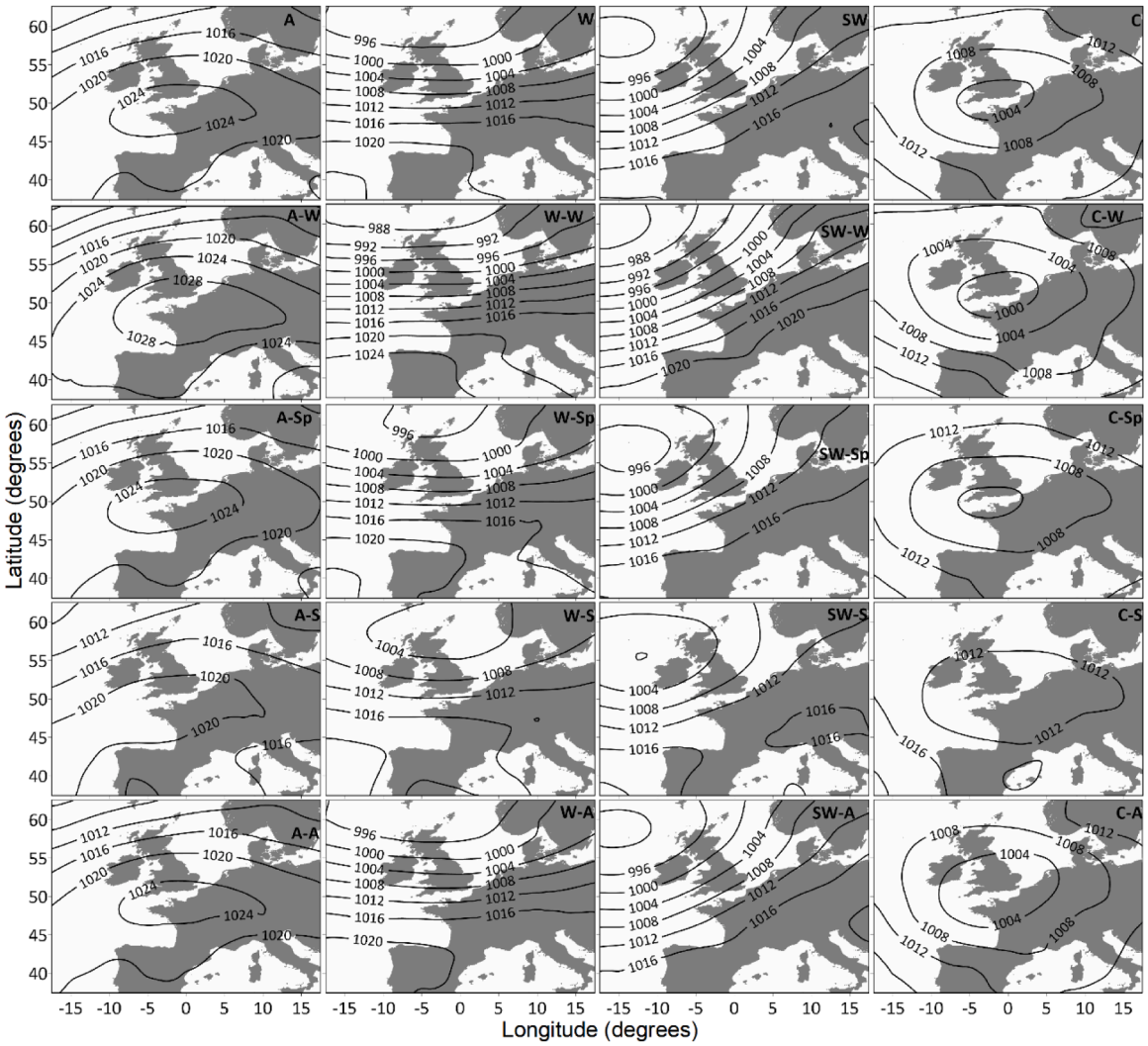

Fig. 6. Pressure fields (hPa) for specific types with all the observations in the first row and for seasons in the rest (winter, W; spring, Sp; summer, S; autumn, A).

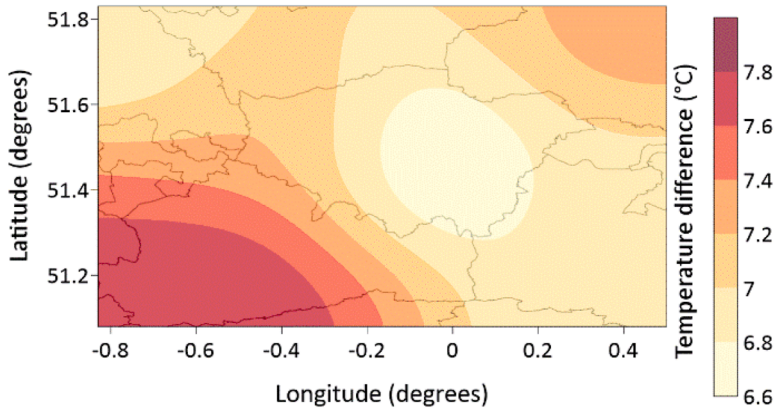

Fig. 7. Temperature difference obtained from smoothing daily differences.

An analogous result is observed for T_{min} in Fig. S5. For this variable, the increase was positive and statistically significant for A type in an area covering from the city centre to the south of the region studied.

3.5. $T_{0.9}$ trend

Table 2 presents the global results when daily temperatures higher than $T_{0.9}$ are inside the region, i.e. the urban heat island does not touch the region limits. Results for the most frequent types are also presented. The increase is about 0.9 °C/10 years for T_{max} and 0.3 °C/10 years for T_{min}., with the highest values being for A type, i.e., around 1 and 0.5 °C/10 years, respectively. However, the surface fraction decreased at a rate of around 0.6 and 0.5 %/10 years for T_{max} and T_{min}, respectively, with the highest surface decrease being for A type, about 0.8 %/10 years for

Table 1
Average temperatures and standard deviations following weather type and season in the region, with mean temperatures above $T_{0.9}$, denoted as T_{in}, and outside this region, denoted as T_{out}.

Temperature	Type	Season	T_{in} (°C)	T_{out} (°C)
T_{max}			15.18±0.04	14.7 ± 0.3
	A		16.50±0.04	15.9 ± 0.3
		W	7.93±0.04	7.4 ± 0.2
		Sp	15.89±0.04	15.3 ± 0.3
		S	23.54±0.04	22.9 ± 0.3
		A	16.43±0.04	16.0 ± 0.2
	W		14.17±0.04	13.7 ± 0.3
		W	10.08±0.04	9.7 ± 0.2
		Sp	13.56±0.04	13.0 ± 0.3
		S	20.51±0.04	19.9 ± 0.4
		A	14.97±0.04	14.5 ± 0.3
	SW		15.01±0.04	14.5 ± 0.3
		W	10.74±0.03	10.3 ± 0.2
		Sp	14.73±0.05	14.1 ± 0.4
		S	21.53±0.06	20.7 ± 0.5
		A	16.27±0.04	15.7 ± 0.3
	C		14.05±0.04	13.6 ± 0.3
		W	6.05±0.04	5.6 ± 0.3
		Sp	13.24±0.04	12.8 ± 0.3
		S	21.15±0.05	20.6 ± 0.3
		A	14.03±0.04	13.6 ± 0.3
T_{min}			8.46±0.05	7.6 ± 0.4
	A		7.99±0.07	6.9 ± 0.5
		W	2.69±0.06	1.7 ± 0.4
		Sp	6.19±0.07	5.0 ± 0.5
		S	13.15±0.07	12.0 ± 0.5
		A	8.42±0.07	7.2 ± 0.5
	W		8.88±0.04	8.2 ± 0.3
		W	6.05±0.04	5.4 ± 0.3
		Sp	7.38±0.04	6.7 ± 0.3
		S	13.63±0.05	12.9 ± 0.3
		A	9.98±0.04	9.3 ± 0.3
	SW		9.70±0.04	9.0 ± 0.3
		W	6.52±0.04	5.9 ± 0.2
		Sp	8.58±0.04	7.7 ± 0.3
		S	14.43±0.05	13.6 ± 0.3
		A	11.07±0.04	10.3 ± 0.3
	C		8.71±0.04	7.9 ± 0.3
		W	3.14±0.04	2.4 ± 0.3
		Sp	7.28±0.04	6.5 ± 0.3
		S	14.41±0.05	13.6 ± 0.4
		A	9.08±0.04	8.3 ± 0.3

T_{max}, whereas the decrease was about 0.6 %/10 years for T_{min} for SW type.

When harmonic terms are added to the linear fit following Eq. (17), temperature change is divided into two parts. One corresponds to the direct linear evolution given by the B coefficient, which was more moderate, 0.5 and 0 °C/10 years for T_{max} and T_{min}, respectively. The second term corresponds to the amplitude evolution, which is presented in the last column, as a result of a combination of harmonic terms. The correlation coefficients are quite satisfactory, and noticeable values of the amplitude change are around 0.4 and 0.2 °C/10 years for T_{max} and T_{min}, respectively.

4. Discussion

4.1. The London heat island

Wilby (2003) used two sites in London –Wisley and St. James– to establish the urban heat island. However, the current research considers a network of values that covers the city and its surrounding areas. Consequently, the representativeness of the values increases. Zhou et al. (2016) divided the Greater London area into two regions –the city cluster and its belt– and calculated urban heat island intensity from the two regions. This temperature contrast was higher during the night, reaching 1.6 °C, and lower during the day, around 0.8 °C or even lower.

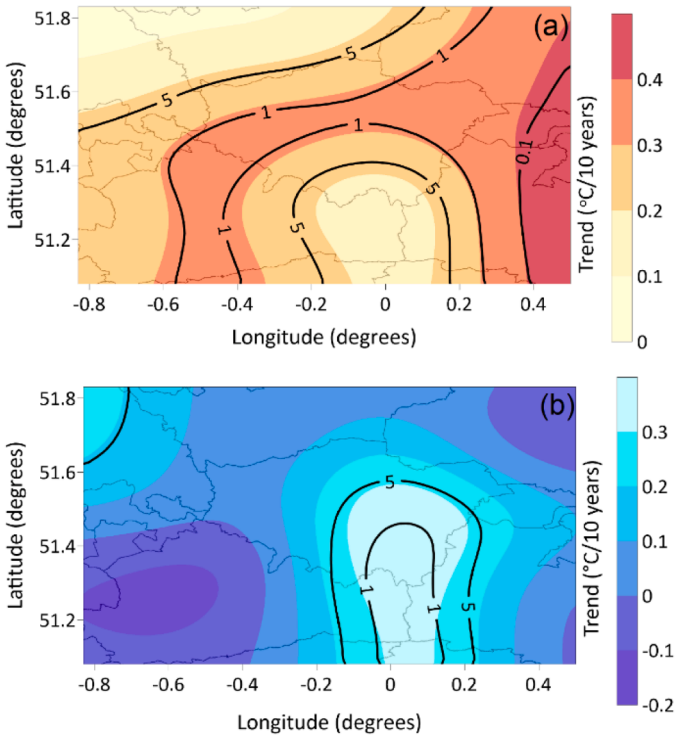

Fig. 8. Trend for T_{max} (a) and T_{min} (b). Black lines correspond to the significance levels (%) of the correlation coefficient.

In the current paper, a wider region is studied. Temperature contrast is similar during the night, but higher during the day. Safarrad et al. (2022) calculated the night-time urban heat island in several European cities in 2019 and 2020, dividing the cities into several areas following heat island intensity. In London city centre, this intensity reached 4 °C, and the influence of the pandemic was seen to be slight, since surface decreased for the highest intensities, and urban heat island intensity was around 1 °C lower at peripheral sites of the city.

The current study considers smoothed temperatures, such that contrasts between the city centre and its surroundings are consequently small. This contrast is only above 1 °C for specific situations. Guha et al. (2018) considered Landsat 8 data and obtained differences slightly above 3 °C between the hottest areas of Florence and Naples, Italy, and their boundaries. The hottest and coldest sites inside the city may be separated due to the high resolution of these images. However, the London analysis in this paper focuses on the contrast between the city and the surrounding area. Boccalatte et al. (2023) considered urban heat island intensity as the positive difference between urban and rural air temperatures, which were modelled, and applied it in the Canton of Geneva, Switzerland, where it ranged from 1.7 to 2.2 °C. Geng et al. (2023) analysed the urban heat island with satellite data in 253 Chinese cities in five climate zones and obtained values between −2.59 and 6.20 °C. These examples indicate the varied values that can be obtained depending on each city's specific features.

City response to the diurnal cycle has been investigated in some studies. Zargari et al. (2024) considered satellite images to study the Tehran heat island, and obtained an urban heat island during the night, but an urban cool island during the day. Díaz-Chávez et al. (2024) studied urban heat island intensity in five coastal cities in northern Colombia with Landsat images, using a numerical model. They obtained higher values for the urban heat island during the day compared to those obtained during the night. In the current study, the temperature contrast in the region analysed was slightly higher for T_{min} (night) versus T_{max} (day). However, the main difference was the surface of high temperatures, which was considerably higher during the day. Hence, a

Table 2
$T_{0.9}$ trend calculation by linear fit and with a harmonic model. Values are accompanied by standard deviations.

Temperature and type	Data (%)	$T_{0.9}$ trend (°C/10 years)	Surface fraction trend (%/10 years)	A* (°C)	B* (°C/10 years)	C* (°C)	D* (°C)	E* (°C/10 years)	F* (°C/10 years)	r	Amplitude trend (°C/10 years)
T_{max} (all types)	34.8	0.86±0.11	−0.64±0.05	15.00 ±0.10	0.54±0.06	−7.02 ±0.15	−2.45 ±0.14	−0.46 ±0.08	−0.12 ±0.08	0.867	0.4049±0.0006
A	9.6	1.1 ± 0.2	−0.76±0.10	15.41 ±0.17	0.54±0.09	−8.4 ± 0.2	−2.0 ± 0.2	−0.08 ±0.13	0.09±0.13	0.914	0.06449 ±0.00011
W	3.3	0.1 ± 0.3	−0.6 ± 0.2	15.3 ± 0.2	0.05±0.13	−5.2 ± 0.3	−1.6 ± 0.3	−0.09 ±0.17	−0.2 ± 0.2	0.890	0.1713±0.0005
SW	3.1	0.0 ± 0.3	−0.21±0.18	16.0 ± 0.3	0.22±0.16	−5.2 ± 0.4	−2.5 ± 0.3	−0.3 ± 0.2	0.12±0.19	0.870	0.2014±0.0006
C	2.1	−0.1 ± 0.5	−0.7 ± 0.2	14.3 ± 0.4	0.2 ± 0.3	−7.6 ± 0.7	−3.6 ± 0.6	−0.4 ± 0.4	0.7 ± 0.4	0.857	0.221±0.006
T_{min} (all types)	47.0	0.26±0.07	−0.48±0.04	9.08 ±0.09	−0.07 ±0.04	−4.28 ±0.12	−2.51 ±0.12	−0.20 ±0.06	−0.12 ±0.06	0.782	0.235324 ±0.000011
A	11.5	0.53±0.15	−0.50±0.07	8.02 ±0.18	0.06±0.09	−5.0 ± 0.2	−2.3 ± 0.3	0.01±0.12	−0.09 ±0.13	0.809	0.03320 ±0.00010
W	4.7	0.17±0.18	−0.38±0.11	9.8 ± 0.2	0.05±0.13	−3.3 ± 0.3	−1.8 ± 0.3	−0.22 ±0.17	−0.08 ±0.18	0.737	0.23719 ±0.00002
SW	5.4	0.08±0.17	−0.62±0.11	10.9 ± 0.2	−0.27 ±0.12	−3.5 ± 0.3	−2.1 ± 0.3	−0.13 ±0.16	−0.17 ±0.18	0.747	0.20632 ±0.00009
C	3.8	0.2 ± 0.3	−0.52±0.13	8.7 ± 0.3	0.06±0.15	−5.8 ± 0.4	−3.1 ± 0.4	−0.2 ± 0.2	0.1 ± 0.2	0.858	0.1125±0.0003

* Model: $T_{0.9}$=A+Bt+C cos(2πt/T)+D sin(2πt/T)+E t cos(2πt/T)+F t sin(2πt/T), t is time, and T is the period of one year.

contraction of the urban heat island was observed in the transition from day to night, and an expansion was seen for the transition from night to day.

Qin et al. (2024) investigated research trends for mitigating the urban heat island. They considered eight main categories. Vegetation and shade was the first category, which involved green roofs and walls. This was followed by urban planning and design, where park development is included. However, permeable pavements, such as cool roofs, or natural ventilation are also of substantial interest. Alizadehtazi et al. (2024) quantified the green roof impact in New York City to be slightly below 1 °C. Similar values were obtained with green walls (Ornam et al., 2024), although their maintenance cost may prove to be a drawback. However, Kim et al. (2024) indicated that trees are two or three times more effective at reducing local air temperature than green roofs or walls. Urban vegetation forms urban cooling islands, which were investigated by Wang et al. (2023) in China, with their average being 2.47 °C, with the largest values in small cities and the temperate continental climate zone. The average cooling magnitude of urban parks was around 2 °C in Melbourne, Australia (Algretawee, 2023). Moreover, the cooling effect of urban water bodies –known as urban blue spaces– should not be ignored. Zhou et al. (2024) observed this effect by a river in Suzhou, China, where the cooling effect was mainly observed in summer. Finally, Kang et al. (2024) concluded that single-centre cities and cities with a high continuous urban spatial structure are linked with increased intensities of urban heat islands. Consequently, urban development should be directed towards avoiding this problem. Current research for London reveals that the urban heat island effect is weak and that the area where such measures should be implemented is the city centre, since the temperature distribution is symmetrically distributed around it, especially during the night.

4.2. Weather types

Stations utilised by Wilby (2003) were used by Wilby et al. (2011) together with Lamb weather types for London. Urban heat island intensity was between 1 and 4 °C, with the authors distinguishing between summer and annual values. The contrast between these values and the values obtained in the current analysis may be attributed to the smoothing process wherein averages are calculated. De Luca et al. (2019) considered a network centred on the British Isles to determine Lamb weather types. They introduced the description of the eight frequent types and obtained A, C and W types as the most frequent. The Wilby et al. (2011) method was used to determine urban heat island intensity, with the authors observing the correlation between intense urban heat island summer events and the anticyclonic type.

Pérez et al. (2024) studied the London pollution island under Lamb weather types with five years of measurements, although seasonal analysis was not presented. Weather type distribution in the current research with 33 years of data is analogous. In that analysis, similar shapes were observed for the urban pollution island under different weather types, with the concentration values being different. However, the urban heat island shape is linked to weather type for T_{max}, since it is confined to the region studied for A and C types. However, the urban heat island was insensitive to weather type for T_{min} and was confined to the city centre.

Additional papers consider the relationship between the urban heat island and weather types, which may be determined by different procedures. Hardin et al. (2018) analysed different stations inside and outside cities in northeast US to calculate urban heat island intensity. Moreover, they used a weather type classification developed by Sheridan (2002). This is a hybrid scheme composed of manual and automated methods that considers seven weather types. Arnds et al. (2017) analysed the mean nocturnal urban heat island of Hamburg, and highlighted the influence of several meteorological variables such as wind speed –especially in autumn– cloud cover in winter, and relative humidity in spring and summer. Moreover, the influence of objective weather types was also underlined, although their seasonal influence was unsteady due to their strongly variable frequency. These objective weather types were determined by the German Meteorological Service (2024), with the classification being made up of 40 weather types. Petrou et al. (2023) used ten weather types, which were determined using statistical procedures and are described by four variables, i.e., temperature, wind direction, specific humidity, and cloud cover. Annual cycles of these types are presented together with the contrast between urban and rural temperatures for the Attica region, Greece. The highest contrasts were about 7 °C during summer daytime, whereas they were slightly higher during summer night-time. Colangelo et al. (2022) used weather types based on a taxonomic scheme centred in Italy. They considered the daily thermal range in different local climate zones, which were defined by building density and vegetation (Stewart & Oke, 2012), under anticyclonic and cyclonic conditions. Lee (2015, 2020) developed a weather type classification based on temperature and

humidity, which may be used from gridded meteorological variables. Eleven weather types are defined, with two being transitional weather types that correspond to front passages. Kassomenos et al. (2022) applied this classification to two cities in Greece –Athens and Thessaloniki– and obtained an increase in warm group frequency and a decrease in cold group frequency in Athens. Moreover, right-skewed distributions of the urban-suburban temperature difference were obtained in Athens during the day. However, a softer skewness was observed in Thessaloniki. Contrasts between urban and rural environments were small. However, the main contrasts were observed for the highest temperatures, since the most frequent difference was 2 °C for Athens during the day, and 6 °C for Thessaloniki during both day and night. Hartmann et al. (2023) studied the urban heat island in Wurzburg, Germany. The highest difference between the inner city and the outskirts was 8.2 °C. This effect heightened in summer when anticyclonic weather types prevailed over Central Europe. Moreover, the cooling effect of urban trees was estimated to be about 2 °C, although it may be half of this value when trees are affected by water stress. High values were observed in the current analysis for the London heat island for minimum temperature under the anticyclonic type, although there is no acute seasonal contrast, since intensity ranged from 1 °C in winter to 1.2 °C in spring and summer.

Zakarin et al. (2022) studied stagnant conditions at Almaty, Kazakhstan. They pointed out the strong dependence of urban heat islands on wind conditions, and found heat islands to be cooler during the night than during the day due to the katabatic wind from the nearby mountains. The London urban heat island extends along the river valley, although its shape is more acute during the day. Noticeable orographic features are not observed. However, directional patterns do impact the urban heat island extension. Consequently, corrective actions could be implemented in the east of the city to reduce airflow influence. Anjos et al. (2020) studied the urban heat island at Londrina, Brazil, a mid-sized city with around 600,000 inhabitants, under different synoptic patterns and obtained the largest intensities during the night under anticyclone conditions, whereas overcast and rainy conditions were linked to the lowest intensities. These conditions are associated with the passage of troughs, cold fronts and complex mesoscale systems. Since these conditions are not steady, they are excluded from the usual weather-type classifications. This is one restriction of Lamb weather types. However, the most representative pattern for London –type A– provides an accurate representation of the urban heat island vis-à-vis planning future city development.

4.3. Temperature trend

Bassett et al. (2021) considered urban heat island intensity in London with observations from the weather station in St James' Park as well as those at nearby sites from ECMWF ERA5 atmospheric reanalysis. The highest intensity was obtained in April, which was about 2.5 °C, and the lowest was observed in December, which was around 1.7 °C. The temperature contrast in this study agrees with the one presented in that paper. Moreover, the authors indicated no significant changes in urban heat island intensity over the period 1950 to 2019. Badugu et al. (2023) studied the urban heat island at Tiruchirappalli, India, and obtained an urban heat island at night. The temperature increase was 0.17 °C in 10 years. Moreover, they identified a hot spot outside the urban area –which was linked to industry– and some cold spots within the rural area. This study presents a similar temperature increase –around 0.2–0.3 °C/10 years– in the city centre. Moreover, the $T_{0.9}$ trend was 0.86 °C/10 years for T_{max}, whereas it was 0.26 °C/10 years for T_{min} for all weather types. Neither cold nor hot spots were observed, although an area in the south of the city stood out due to its noticeable T_{min} trend of around 0.3 °C/10 years.

Orkomi and Ameri (2024) studied the urban heat island in a mid-sized city –Rasht in Iran– and obtained an increasing trend in hot seasons over the last 20 years, whereas this island remained steady in cold seasons. Zhao et al. (2024) investigated the urban heat island in the Yangtze River Delta, China. Despite the high land surface temperature at the urban cores, some cities with high urbanization levels showed a cooling trend due to urban renewal by vegetation restoration. Díaz-Chávez et al. (2024) reported an evolution in urban heat island intensity that was attributed to the growth of urban areas and the densification of built-up areas in five coastal cities in northern Colombia. They suggested procedures such as the construction of green areas and roofs, the use of materials with low heat absorption and high reflectance, and the development of linear parks and green corridors. Huang et al. (2024) observed an intensifying trend of summer heat island or cool island effects in six Chinese cities over the period 2013–2023, which was attributed to planning layout and urban expansion, although other factors –such as population density– were seen to have a minimal impact. Deng et al. (2024) analysed 717 cities worldwide after 2010 under varied climates and with urban areas of over 100 km^2. They found a global decreasing trend of the urban heat island during the day and night, although significant disparities were also found. Moreover, a noticeable cooling effect of vegetation was evident in smaller arid cities.

The heat island is the urban response to urban activity. How it evolves depends on how the climate evolves as well as on how urban activity evolves. However, despite the specific and varied evolutions found worldwide, the current analysis does not show any specific trend for London city centre. Consequently, this analysis suggests that climate change determines the temperature evolution in the region studied. Masucci et al. (2013) indicated that London street density barely evolved over the period 1990–2010. In their review paper, Lai et al. (2019) concluded that changes in urban geometry as well as the introduction of vegetation, cool surfaces and water bodies can reduce air temperature by around 2 °C in summer. City centre activities could be spatially distributed to decrease the urban heat island effect since a lower activity density will reduce the associated traffic. Cheng et al. (2006) suggested changes in urban design and considered three examples. In the first, they recommended scattered layouts for blocks instead of uniform arrays. In the second example, the availability of more open space with higher buildings is preferable vis-à-vis lower buildings and higher site coverage. The third example is a vertical random layout, which is encouraged in preference to a uniform vertical distribution. Deng et al. (2023) considered three alternative designs. The first corresponds to freestanding plots, which are large-scale building complexes where a super high-rise tower is on a multi-storey podium. The second urban form is for scattered plots where a more open layout is observed from several high-rise towers without podiums. The third urban form is for the enclosed plot where an inner courtyard is surrounded by buildings. These types were identified in the central area of Nanjing, China, with the maximum air temperature being for the freestanding plot. This temperature was about 4 °C higher at midday than the temperature for the scattered plot. However, this temperature was about 1 °C higher than the temperature for the enclosed plot, which presented the lowest value.

Green areas could be also increased. One key feature is green roofs, which decrease rainwater runoff and reduce the heat island effect (Salih et al., 2022). The cooling effect of urban greenery has been analysed at three scales: the block scale, such as streets, the neighbourhood scale, and the city scale (Licón-Portillo et al., 2024). The minimum effect was reached at the city scale, and the maximum at the neighbourhood scale, although differences between results in these scales are small, and were between around 0.5 and 2.5 °C. Noticeable changes of around 1.7 °C in the urban heat island were reached in India with small changes in vegetation (Bhanage et al., 2023). A contrast of about 2 °C between blue-green spaces and non-blue-green spaces was found to be the cooling effect in Bhubaneswar, India (Pritipadmaja et al., 2023). Thermal mitigation thanks to city afforestation was investigated by Wu et al. (2024) in China and was found to lead to reductions in urban surface temperature of about 0.1 °C with a 1 % increase in vegetation coverage, although a temperature increase was sometimes observed in rural areas

with increased vegetation. Taylor et al. (2024) recorded lower urban temperatures of around 0.8 °C for maximum temperatures and 2 °C for minimum temperatures during heatwaves for areas of London with high canopy coverage compared to those with low canopy coverage. Traffic restrictions, and even establishing zero emission zones, could be among some of the measures adopted to decrease the urban heat island effect. Finally, burying traffic could be a measure taken to increase green zone coverage and thereby cut air pollution concentration. The Superblock model –where streets are replaced by green axes– is now being implemented in Europe as a response to prevent the negative impacts of public transport, air pollution, noise and urban heat islands (Nieuwenhuijsen et al., 2024). All of this previous experience reveals that designers are necessary partners to create cooler cities using microclimate information (Lin et al., 2022).

5. Conclusions

This analysis of maximum and minimum temperatures in the London region over a period of 33 years increases the number of studies addressing the urban heat island during the day and night. It reveals similar values of urban heat island intensity –around 1.4 °C. However, the surface of the urban heat island for the maximum temperature extended along the valley, whereas the minimum temperature was closely confined to the city centre. A contraction of the urban heat island extension is observed in the transition from day to night. A restrictive limit, such as temperature for an urban heat island index equal to 0.9, should be considered in order to obtain a defined urban heat island in the region studied.

One noticeable feature of the current analysis when compared to previous studies is the focus on the relationship between the urban heat island and the synoptic pattern. The anticyclonic type was prominent, followed by two directional types –westerly and south-westerly types– which were characterised by strong winds in winter. Cyclonic type frequency was also noticeable and its wind speed was low, especially in summer. In contrast, the smallest frequencies were for the hybrid cyclonic types.

Among the most frequent types, directional ones presented mild values for both temperatures in winter and early spring and even in summer for the maximum temperature, which may be attributed to the transport of oceanic air masses. The lowest values in winter were for cyclonic situations for the maximum temperature and anticyclonic situations for the minimum temperature.

Another noticeable feature of this research is the reported influence of the synoptic pattern on the urban heat island shape. Among the most frequent weather types, both directional types –westerly and south-westerly –provided a noticeably extended urban heat island for the maximum temperature, whereas it was closely confined to the city centre for the minimum temperature.

The difference between the two temperatures was around 6.8 °C and was confined to the city centre, whereas the highest contrast was about 1 °C greater, and was observed outside the city in the SW.

Temperature trends were calculated and values of 0.2–0.3 °C/10 years were obtained for the city centre, although an urban heat island was not observed for the temperature trend, with this result being an additional feature of this research. Moreover, satisfactory agreements were obtained for the harmonic models used to fit specific temperatures such as this for an urban heat island index equal to 0.9.

The main limitations of the current analysis stem from the calculation procedure. Hotspots in the city are omitted since the smoothing procedure is geared towards calculating the urban heat island shape. Moreover, the annual cycle is only considered in the trend calculation. This procedure should be considered as a first approach, since lower frequency evolutions are omitted. Another limitation comes from the procedure itself. Although the period used is long enough, seasonal analyses divide the original series, and trend results must be taken with caution, as the statistical significance of the correlation coefficient has shown.

Since the current database includes Europe, North Africa, and the Middle East, similar analyses may be carried out for all large enough cities in this region. Such studies would allow the urban heat island to be compared under varied climates and urban structures. Moreover, the results to emerge from such research would help urban planners to mitigate this effect in cities that are experiencing rapid and negative development, since the urban heat island shape may be determined under the most frequent synoptic types.

Further research should consider urban heat island features under specific conditions, such as cold or heat waves, as well as air trajectories linked to these situations. This analysis could provide information about the transport of cold or hot air, source regions, corresponding weather patterns, and their impact on this urban island. Moreover, the urban heat island is integrated into the urban meteorology island. Hence, the city's impact on other meteorological variables should be explored. Finally, the relationship between the urban meteorology island and the urban pollution island is a field that is open to future research, and one which might help to control air pollution and to define city development and expansion.

Funding

This research received no external funding.

Data availability

Temperature data were obtained from Thiemig et al. (2022). The web page was presented at the data availability section, https://data.jrc.ec.europa.eu/dataset/0bd84be4-cec8-4180-97a6-8b3adaac4d26. Moreover, pressure data were obtained from https://psl.noaa.gov that is considered at the data availability section. Supplementary materials are results of calculations.

CRediT authorship contribution statement

Isidro A. Pérez: Writing – original draft, Software, Methodology, Investigation. **M. Ángeles García:** Writing – review & editing. **Saeed Rasekhi:** Writing – review & editing. **Fatemeh Pazoki:** Writing – review & editing. **Beatriz Fernández-Duque:** Writing – review & editing.

Declaration of competing interest

The authors declare that they have no known competing financial interests or personal relationships that could have appeared to influence the work reported in this paper.

Supplementary materials

Supplementary material associated with this article can be found, in the online version, at doi:10.1016/j.scs.2024.105743.

References

Algretawee, H. (2023). The effect of graduated urban park size on park cooling island and distance relative to land surface temperature (LST). *Urban Climate, 45*, Article 101255. https://doi.org/10.1016/j.uclim.2022.101255

Alizadehtazi, B., Stolper, J., Singh, K., & Montalto, F. A. (2024). Microclimatic implications of a large-scale green roof and high-rise redevelopment in New York City. *Building and Environment, 250*, Article 111113. https://doi.org/10.1016/j.buildenv.2023.111113

Alonso, M. S., Fidalgo, M. R., & Labajo, J. L. (2007). The urban heat island in Salamanca (Spain) and its relationship to meteorological parameters. *Climate Research, 34*(1), 39–46. https://doi.org/10.3354/cr034039

Anjos, M., Targino, A. C., Krecl, P., Oukawa, G. Y., & Braga, R. F. (2020). Analysis of the urban heat island under different synoptic patterns using local climate zones. *Building and Environment, 185*, Article 107268. https://doi.org/10.1016/j.buildenv.2020.107268

Arnds, D., Böhner, J., & Bechtel, B. (2017). Spatio-temporal variance and meteorological drivers of the urban heat island in a European city. *Theoretical and Applied Climatology, 128*(1-2), 43–61. https://doi.org/10.1007/s00704-015-1687-4

Badugu, A., Arunab, K. S., Mathew, A., & Sarwesh, P. (2023). Spatial and temporal analysis of urban heat island effect over Tiruchirappalli city using geospatial techniques. *Geodesy and Geodynamics, 14*(3), 275–291. https://doi.org/10.1016/j.geog.2022.10.004

Bala, R., Yadav, V. P., Kumar, D. N., & Prasad, R. (2024). Quantification of surface urban heat island intensity using MODIS satellite imagery in different Indian cities. *Journal of the Indian Society of Remote Sensing, 52*(2), 327–341. https://doi.org/10.1007/s12524-024-01810-8

Bassett, R., Janes-Bassett, V., Phillipson, J., Young, P. J., & Blair, G. S. (2021). Climate driven trends in London's urban heat island intensity reconstructed over 70 years using a generalized additive model. *Urban Climate, 40*, Article 100990. https://doi.org/10.1016/j.uclim.2021.100990

Bhanage, V., Kulkarni, S., Sharma, R., Lee, H. S., & Gedam, S. (2023). Enumerating and modelling the seasonal alterations of surface urban heat and cool island: A case study over Indian cities. *Urban Science, 7*(2), Article 38. https://doi.org/10.3390/urbansci7020038

Boccalatte, A., Fossa, M., Thebault, M., Ramousse, J., & Ménézo, C. (2023). Mapping the urban heat island at the territory scale: An unsupervised learning approach for urban planning applied to the Canton of Geneva. *Sustainable Cities and Society, 96*, Article 104677. https://doi.org/10.1016/j.scs.2023.104677

Chau, N. H. (2019). Estimation of air temperature using smartphones in different contexts. *Journal of Information and Telecommunication, 3*(4), 494–507. https://doi.org/10.1080/24751839.2019.1634869

Cheng, V., Steemers, K., Montavon, M., & Compagnon, R. (2006). Urban form, density and solar potential. In *PLEA 2006 - 23rd International Conference on Passive and Low Energy Architecture, Conference Proceedings* (pp. I701–I706).

Cetin, M., Ozenen Kavlak, M., Senyel Kurkcuoglu, M. A., Bilge Ozturk, G., Cabuk, S. N., & Cabuk, A. (2024). Determination of land surface temperature and urban heat island effects with remote sensing capabilities: the case of Kayseri, Türkiye. *Natural Hazards, 120*(6), 5509–5536. https://doi.org/10.1007/s11069-024-06431-5

Colangelo, G., Sanesi, G., Mariani, L., Parisi, S. G., & Cola, G. (2022). A circulation weather type analysis of urban effects on daily thermal range for Milan (Italy). *Atmosphere, 13*(9), Article 1529. https://doi.org/10.3390/atmos13091529

De Luca, P., Harpham, C., Wilby, R. L., Hillier, J. K., Franzke, C. L. E., & Leckebusch, G. C. (2019). Past and projected weather pattern persistence with associated multi-hazards in the British Isles. *Atmosphere, 10*(10), Article 577. https://doi.org/10.3390/atmos10100577

Deng, J. Y., He, Y., & Dai, M. (2023). Evaluation of the outdoor thermal environment for three typical urban forms in Nanjing, China. *Building and Environment, 238*, Article 110358. https://doi.org/10.1016/j.buildenv.2023.110358

Deng, X., Yu, W., Shi, J., Huang, Y., Li, D., He, X., Zhou, W., & Xie, Z. (2024). Characteristics of surface urban heat islands in global cities of different scales: Trends and drivers. *Sustainable Cities and Society, 107*, Article 105483. https://doi.org/10.1016/j.scs.2024.105483

Díaz-Chávez, L., Melendez-Surmay, R., & Arregocés, H. A. (2024). Urban heat island intensity in coastal cities of northern Colombia using Landsat data and WRF/UCM model. *Case Studies in Chemical and Environmental Engineering, 9*, Article 100617. https://doi.org/10.1016/j.cscee.2024.100617

Donnelly, A., Misstear, B., & Broderick, B. (2011). Application of nonparametric regression methods to study the relationship between NO_2 concentrations and local wind direction and speed at background sites. *Science of the Total Environment, 409*(6), 1134–1144. https://doi.org/10.1016/j.scitotenv.2010.12.001

Elsevier. (2024) https://www.elsevier.com/products/scopus. Accessed February 15, 2024.

Fernández-Duque, B., Pérez, I. A., García, M. A., Pardo, N., & Sánchez, M. L. (2019). Annual and seasonal cycles of CO_2 and CH_4 in a Mediterranean Spanish environment using different kernel functions. *Stochastic Environmental Research and Risk Assessment, 33*(3), 915–930. https://doi.org/10.1007/s00477-019-01655-5

Fu, X., Yao, L., & Sun, S. (2022). Accessing the heat exposure risk in Beijing–Tianjin–Hebei region based on heat island footprint analysis. *Atmosphere, 13*(5), Article 739. https://doi.org/10.3390/atmos13050739

Geng, X., Zhang, D., Li, C., Yuan, Y., Yu, Z., & Wang, X. (2023). Impacts of climatic zones on urban heat island: Spatiotemporal variations, trends, and drivers in China from 2001–2020. *Sustainable Cities and Society, 89*, Article 104303. https://doi.org/10.1016/j.scs.2022.104303

German Meteorological Service (2024). https://www.dwd.de/EN/ourservices/wetterlagenklassifikation/wetterlagenklassifikation.html. Accessed February 15, 2024.

Guan, Y., Quan, J., Ma, T., Cao, S., Xu, C., & Guo, J. (2023). Identifying major diurnal patterns and drivers of surface urban heat island intensities across local climate zones. *Remote Sensing, 15*(20), Article 5061. https://doi.org/10.3390/rs15205061

Guha, S., Govil, H., Dey, A., & Gill, N. (2018). Analytical study of land surface temperature with NDVI and NDBI using Landsat 8 OLI and TIRS data in Florence and Naples city, Italy. *European Journal of Remote Sensing, 51*(1), 667–678. https://doi.org/10.1080/22797254.2018.1474494

Hamed Fahmy, A., Amin Abdelfatah, M., & El-Fiky, G. (2023). Investigating land use land cover changes and their effects on land surface temperature and urban heat islands in Sharqiyah Governorate, Egypt. *Egyptian Journal of Remote Sensing and Space Science, 26*(2), 293–306. https://doi.org/10.1016/j.ejrs.2023.04.001

Hardin, A. W., Liu, Y., Cao, G., & Vanos, J. K. (2018). Urban heat island intensity and spatial variability by synoptic weather type in the northeast U.S. *Urban Climate, 24*, 747–762. https://doi.org/10.1016/j.uclim.2017.09.001

Hartmann, C., Moser-Reischl, A., Rahman, M. A., Franceschi, E., von Strachwitz, M., Pauleit, S., Pretzsch, H., Rötzer, T., & Paeth, H. (2023). The footprint of heat waves and dry spells in the urban climate of Würzburg, Germany, deduced from a continuous measurement campaign during the anomalously warm years 2018–2020. *Meteorologische Zeitschrift, 32*(1), 49–65. https://doi.org/10.1127/metz/2023/1151

Henning, B., & Dorling, D. (2024). Inequalities in London. http://london.worldmapper.org/analysis/inequality-in-london/(accessed 16 July 2024).

Hu, J., Yang, Y., Zhou, Y., Zhang, T., Ma, Z., & Meng, X. (2022). Spatial patterns and temporal variations of footprint and intensity of surface urban heat island in 141 China cities. *Sustainable Cities and Society, 77*, Article 103585. https://doi.org/10.1016/j.scs.2021.103585

Huang, Q., & Lu, Y. (2018). Urban heat island research from 1991 to 2015: A bibliometric analysis. *Theoretical and Applied Climatology, 131*(3-4), 1055–1067. https://doi.org/10.1007/s00704-016-2025-1

Huang, M., Zhong, S., Mei, X., & He, J. (2024). Spatiotemporal patterns in the urban heat island effect of several contemporary and historical Chinese "stove cities". *Sustainability, 16*(7), Article 3091. https://doi.org/10.3390/su16073091

Jaiswal, N., Deb, S. K., Panda, S. K., Mandal, A. K., Khan, A. W., & Kishtawal, C. M. (2023). Estimation of intra-urban thermal variability in Ahmedabad city using moving vehicle transects. *Journal of Earth System Science, 132*, Article 41. https://doi.org/10.1007/s12040-023-02063-8

Jenkinson, A. F., & Collison, F. P. (1977). *An initial climatology of gales over the North Sea. Synoptic climatology branch memorandum no. 62*. UK: Meteorological office.

Kang, S. W., Lee, M. S., & Jung, J. C. (2024). Analysis of sustainable urban forms for climate change adaptation and mitigation. *Environmental and Sustainability Indicators, 22*, Article 100337. https://doi.org/10.1016/j.indic.2024.100337

Karakuş, C. B. (2019). The impact of land use/land cover (LULC) changes on land surface temperature in Sivas city center and its surroundings and assessment of urban heat island. *Asia-Pacific Journal of Atmospheric Sciences, 55*(4), 669–684. https://doi.org/10.1007/s13143-019-00109-w

Kassomenos, P., Kissas, G., Petrou, I., Begou, P., Khan, H. S., & Santamouris, M. (2022). The influence of daily weather types on the development and intensity of the urban heat island in two Mediterranean coastal metropolises. *Science of the Total Environment, 819*, Article 153071. https://doi.org/10.1016/j.scitotenv.2022.153071

Kim, J., Khouakhi, A., Corstanje, R., & Johnston, A. S. A. (2024). Greater local cooling effects of trees across globally distributed urban green spaces. *Science of the Total Environment, 911*, Article 168494. https://doi.org/10.1016/j.scitotenv.2023.168494

Lai, D., Liu, W., Gan, T., Liu, K., & Chen, Q. (2019). A review of mitigating strategies to improve the thermal environment and thermal comfort in urban outdoor spaces. *Science of the Total Environment, 661*, 337–353. https://doi.org/10.1016/j.scitotenv.2019.01.062

Lamb, H. H. (1972). British Isles weather types and a register of daily sequence of circulation patterns 1861-1971. *Geophysical Memoir, 116*. Meteorological Office, UK.

Lee, C. C. (2015). The development of a gridded weather typing classification scheme. *International Journal of Climatology, 35*(5), 641–659. https://doi.org/10.1002/joc.4010

Lee, C. C. (2020). The gridded weather typing classification version 2: A global-scale expansion. *International Journal of Climatology, 40*(2), 1178–1196. https://doi.org/10.1002/joc.6263

Li, H., Meier, F., Lee, X., Chakraborty, T., Liu, J., Schaap, M., & Sodoudi, S. (2018). Interaction between urban heat island and urban pollution island during summer in Berlin. *Science of the Total Environment, 636*, 818–828. https://doi.org/10.1016/j.scitotenv.2018.04.254

Li, L., Zha, Y., & Zhang, J. (2020). Spatially non-stationary effect of underlying driving factors on surface urban heat islands in global major cities. *International Journal of Applied Earth Observation and Geoinformation, 90*, Article 102131. https://doi.org/10.1016/j.jag.2020.102131

Licón-Portillo, J. A., Martínez-Torres, K. E., Chung-Alonso, P., & Herrera Peraza, E. F. (2024). From block to city scale: Greenery's contribution to cooling the urban environment. *Urban Science, 8*(2), Article 41. https://doi.org/10.3390/urbansci8020041

Lin, J., Li, D., & Brown, R. D. (2022). Microclimatic landscape architecture: From theory to application. *Urban Science, 6*(1), Article 9. https://doi.org/10.3390/urbansci6010009

London Green Cover. (2024). https://apps.london.gov.uk/green-cover/(accessed 16 July 2024).

Masucci, A. P., Stanilov, K., & Batty, M. (2013). Limited urban growth: London's street network dynamics since the 18th century. *PLoS One, 8*, Article e69469. https://doi.org/10.1371/journal.pone.0069469

Mathew, A., Khandelwal, S., & Kaul, N. (2017). Investigating spatial and seasonal variations of urban heat island effect over Jaipur city and its relationship with vegetation, urbanization and elevation parameters. *Sustainable Cities and Society, 35*, 157–177. https://doi.org/10.1016/j.scs.2017.07.013

Matuzko, A. K., & Yakubailik, O. E. (2018). Urban heat island effects over Krasnoyarsk obtained on the basis of Landsat 8 remote sensing data. *IOP Conference Series: Earth and Environmental Science, 211*(1), Article 012010. https://doi.org/10.1088/1755-1315/211/1/012010

Miles, V., & Esau, I. (2020). Surface urban heat islands in 57 cities across different climates in northern Fennoscandia. *Urban Climate, 31*, Article 100575. https://doi.org/10.1016/j.uclim.2019.100575

Mohan, M., Bhati, S., & Sati, A. P. (2022). Urban heat island effect in India: assessment, impacts, and mitigation. In A. Khan, A. Akbari, F. Fiorito, S. Mithun, & D. Niyogi (Eds.), *Global urban heat island mitigation* (pp. 199–250). Amsterdam: Elsevier Inc. https://doi.org/10.1016/B978-0-323-85539-6.00007-X.

Mpakairi, K. S., & Muvengwi, J. (2019). Night-time lights and their influence on summer night land surface temperature in two urban cities of Zimbabwe: A geospatial perspective. *Urban Climate, 29*, Article 100468. https://doi.org/10.1016/j.uclim.2019.100468

Nieuwenhuijsen, M., de Nazelle, A., Pradas, M. C., Daher, C., Dzhambov, A. M., Echave, C., Gössling, S., Iungman, T., Khreis, H., Kirby, N., Khomenko, S., Leth, U., Lorenz, F., Matkovic, V., Müller, J., Palència, L., Pereira Barboza, E., Pérez, K.,

Tatah, L., Tiran, J., Tonne, C., & Mueller, N. (2024). The Superblock model: A review of an innovative urban model for sustainability, liveability, health and well-being. *Environmental Research, 251*, Article 118550. https://doi.org/10.1016/j.envres.2024.118550

NOAA. (2024). https://psl.noaa.gov. (Accessed February 15, 2024).

Orkomi, A. A., & Ameri, M. (2024). Investigating the intensity of urban heat island and the impacts of local climate using verified WRF data: A case study of Rasht, Northern Iran. *Sustainable Cities and Society, 106*, Article 105405. https://doi.org/10.1016/j.scs.2024.105405

Ornam, K., Wonorahardjo, S., & Triyadi, S. (2024). Several façade types for mitigating urban heat island intensity. *Building and Environment, 248*, Article 111031. https://doi.org/10.1016/j.buildenv.2023.111031

Pérez, I. A., García, M. A., Rasekhi, S., & Pazoki, F. (2024). The London pollution island under Lamb weather types. *Urban Climate, 53*, Article 101834. https://doi.org/10.1016/j.uclim.2024.101834

Pérez, I. A., Sánchez, M. L., García, M. A., & Pardo, N. (2017). Trend analysis of CO_2 and CH_4 recorded at a semi-natural site in the northern plateau of the Iberian Peninsula. *Atmospheric Environment, 151*, 24–33. https://doi.org/10.1016/j.atmosenv.2016.11.068

Petrou, I., Kyriazis, N., & Kassomenos, P. (2023). Evaluating the spatial and temporal characteristics of summer urban overheating through weather types in the Attica region, Greece. *Sustainability, 15*(13), Article 10633. https://doi.org/10.3390/su151310633

Pritipadmaja, Garg, R. D., & Sharma, A. K (2023). Assessing the cooling effect of blue-green spaces: Implications for urban heat island mitigation. *Water, 15*(16), Article 2983. https://doi.org/10.3390/w15162983

Qin, Y., Ghalambaz, S., Sheremet, M., Baro, M., & Ghalambaz, M. (2024). Deciphering urban heat island mitigation: A comprehensive analysis of application categories and research trends. *Sustainable Cities and Society, 101*, Article 105081. https://doi.org/10.1016/j.scs.2023.105081

Ravanelli, R., Nascetti, A., Cirigliano, R. V., Di Rico, C., Leuzzi, G., Monti, P., & Crespi, M. (2018). Monitoring the impact of land cover change on surface urban heat island through Google Earth Engine: Proposal of a global methodology, first applications and problems. *Remote Sensing, 10*(9), Article 1488. https://doi.org/10.3390/rs10091488

Reades, J., Lees, L., Hubbard, P., & Lansley, G. (2022). Quantifying state-led gentrification in London: Using linked consumer and administrative records to trace displacement from council estates. *Environment and Planning A, 55*, 810–827. https://doi.org/10.1177/0308518×221135610

Ridwan, Rasyidi, E. S., Syafri, Rahman, R., Okviyani, N., Jumadil, & Ma'Rief, A. A. (2021). Assessment of the relationship between building density and urban heat island using Landsat images in Makassar City. *IOP Conference Series: Earth and Environmental Science, 802*(1), Article 012042. https://doi.org/10.1088/1755-1315/802/1/012042

Safarrad, T., Ghadami, M., & Dittmann, A. (2022). Effects of COVID-19 restriction policies on urban heat islands in some European Cities: Berlin, London, Paris, Madrid, and Frankfurt. *International Journal of Environmental Research and Public Health, 19*(11), Article 6579. https://doi.org/10.3390/ijerph19116579

Salih, K., Saeed, Z. O., & Almukhtar, A. (2022). Lessons from New York high line green roof: Conserving biodiversity and reconnecting with nature. *Urban Science, 6*(1), Article 2. https://doi.org/10.3390/urbansci6010002

Sarker, T., Fan, P., Messina, J. P., Mujahid, N., Aldrian, E., & Chen, J. (2024). Impact of urban built-up volume on urban environment: A case of Jakarta. *Sustainable Cities and Society, 105*, Article 105346. https://doi.org/10.1016/j.scs.2024.105346

Seeberg, G., Hostlowsky, A., Huber, J., Kamm, J., Lincke, L., & Schwingshackl, C. (2022). Evaluating the potential of Landsat satellite data to monitor the effectiveness of measures to mitigate urban heat islands: A case study for Stuttgart (Germany). *Urban Science, 6*(4), Article 82. https://doi.org/10.3390/urbansci6040082

Sheridan, S. C. (2002). The redevelopment of a weather-type classification scheme for North America. *International Journal of Climatology, 22*(1), 51–68. https://doi.org/10.1002/joc.709

Shi, Y., & Zhang, Y. (2022). Urban morphological indicators of urban heat and moisture islands under various sky conditions in a humid subtropical region. *Building and Environment, 214*, Article 108906. https://doi.org/10.1016/j.buildenv.2022.108906

Si, M., Yao, N., Li, Z. L., Liu, X., Tang, B. H., & Nerry, F. (2024). Feasibility of urban–rural temperature difference method in surface urban heat island analysis under non-uniform rural landcover: A case study in 34 major urban agglomerations in China. *Remote Sensing, 16*(7), Article 1232. https://doi.org/10.3390/rs16071232

Stewart, I. D., & Oke, T. R. (2012). Local climate zones for urban temperature studies. *Bulletin of the American Meteorological Society, 93*(12), 1879–1900. https://doi.org/10.1175/BAMS-D-11-00019.1

Sun, Y., Wang, S., & Wang, Y. (2020). Estimating local-scale urban heat island intensity using nighttime light satellite imageries. *Sustainable Cities and Society, 57*, Article 102125. https://doi.org/10.1016/j.scs.2020.102125

Suthar, G., Singhal, R. P., Khandelwal, S., & Kaul, N. (2023). Spatiotemporal variation of air pollutants and their relationship with land surface temperature in Bengaluru, India. *Remote Sensing Applications: Society and Environment, 32*, Article 101011. https://doi.org/10.1016/j.rsase.2023.101011

Taylor, J., Simpson, C., Brousse, O., Viitanen, A.-K., & Heaviside, C. (2024). The potential of urban trees to reduce heat-related mortality in London. *Environmental Research Letters, 19*(5), Article 054004. https://doi.org/10.1088/1748-9326/ad3a7e

Thiemig, V., Gomes, G. N., Skøien, J. O., Ziese, M., Rauthe-Schöch, A., Rustemeier, E., Rehfeldt, K., Walawender, J. P., Kolbe, C., Pichon, D., Schweim, C., & Salamon, P. (2022). EMO-5: A high-resolution multi-variable gridded meteorological dataset for Europe. *Earth System Science Data, 14*(7), 3249–3272. https://doi.org/10.5194/essd-14-3249-2022

Wang, C., Ren, Z., Du, Y., Guo, Y., Zhang, P., Wang, G., … Li, T. (2023). Urban vegetation cooling capacity was enhanced under rapid urbanization in China. *Journal of Cleaner Production, 425*, Article 138906. https://doi.org/10.1016/j.jclepro.2023.138906

Wang, Q., Chen, Y., Lu, X., Chen, G., Li, Z., Cai, M., … Fung, J. C. H. (2024). Urbanization impact on meteorological condition and O_3 concentration under past and future climates scenarios over the Greater Bay Area in Southern China. *Atmospheric Environment, 331*, Article 120585. https://doi.org/10.1016/j.atmosenv.2024.120585

Wilby, R. L. (2003). Past and projected trends in London's urban heat island. *Weather, 58*(7), 251–260. https://doi.org/10.1256/wea.183.02

Wilby, R. L., Jones, P. D., & Lister, D. H. (2011). Decadal variations in the nocturnal heat island of London. *Weather, 66*(3), 59–64. https://doi.org/10.1002/wea.679

Wu, B., Zhang, Y., Wang, Y., He, Y., Wang, J., Wu, Y., Lin, X., & Wu, S. (2024). Mitigation of urban heat island in China (2000–2020) through vegetation-induced cooling. *Sustainable Cities and Society, 112*, Article 105599. https://doi.org/10.1016/j.scs.2024.105599

Xu, L., Cui, S., Tang, J., Nguyen, M., Liu, J., & Zhao, Y. (2019). Assessing the adaptive capacity of urban form to climate stress: A case study on an urban heat island. *Environmental Research Letters, 14*(4), Article 044013. https://doi.org/10.1088/1748-9326/aafe27

Yang, K., Zhou, T., Wang, C., Wang, Z., Han, Q., & Tao, F. (2022). RSEDM: A new rotational-scan exponential decay model for extracting the surface urban heat island footprint. *Remote Sensing, 14*(14), Article 3505. https://doi.org/10.3390/rs14143505

Yao, L., Sun, S., Song, C., Wang, Y., & Xu, Y. (2022). Recognizing surface urban heat 'island' effect and its urbanization association in terms of intensity, footprint, and capacity: A case study with multi-dimensional analysis in Northern China. *Journal of Cleaner Production, 372*, Article 133720. https://doi.org/10.1016/j.jclepro.2022.133720

Zakarin, E., Baklanov, A., Balakay, L., Dedova, T., & Bostanbekov, K. (2022). Modeling of the calm situations in the atmosphere of Almaty. *Asian Journal of Atmospheric Environment, 16*(1), 1–15. https://doi.org/10.5572/ajae.2022.007

Zargari, M., Mofidi, A., Entezari, A., & Baaghideh, M. (2024). Climatic comparison of surface urban heat island using satellite remote sensing in Tehran and suburbs. *Scientific Reports, 14*(1), Article 643. https://doi.org/10.1038/s41598-023-50757-2

Zhao, C., Zhu, H., Zhang, S., Jin, Z., Zhang, Y., Wang, Y., Shi, Y., Jiang, J., Chen, X., & Liu, M. (2024). Long−term trends in surface thermal environment and its potential drivers along the urban development gradients in rapidly urbanizing regions of China. *Sustainable Cities and Society, 105*, Article 105324. https://doi.org/10.1016/j.scs.2024.105324

Zhou, B., Lauwaet, D., Hooyberghs, H., De Ridder, K., Kropp, J. P., & Rybski, D. (2016). Assessing seasonality in the surface urban heat island of London. *Journal of Applied Meteorology and Climatology, 55*(3), 493–505. https://doi.org/10.1175/JAMC-D-15-0041.1

Zhou, D., Xiao, J., Bonafoni, S., Berger, C., Deilami, K., Zhou, Y., Frolking, S., Yao, R., Qiao, Z., & Sobrino, J. A. (2018). Satellite remote sensing of surface urban heat islands: Progress, challenges, and perspectives. *Remote Sensing, 11*(1), Article 48. https://doi.org/10.3390/rs11010048

Zhou, W., Wu, T., & Tao, X. (2024). Exploring the spatial and seasonal heterogeneity of cooling effect of an urban river on a landscape scale. *Scientific Reports, 14*(1), Article 8327. https://doi.org/10.1038/s41598-024-58879-x

Zhou, Z., Nguyen-Xuan, T., Liao, H., Qiu, L., & Im, E. S. (2024). Characterization of temperature and humidity effects on extreme heat stress under global warming and urban growth in the Pearl and Yangtze River Deltas of China. *Weather and Climate Extremes, 44*, Article 100659. https://doi.org/10.1016/j.wace.2024.100659